LITHOS 436–437 (2023) 106980

Contents lists available at ScienceDirect

LITHOS

journal homepage: www.elsevier.com/locate/lithos

Prospective pyroxenite–peridotite mixed mantle source for the northern Carlsberg Ridge

Hang Hu [a,b], Xing Yu [a,b,*], Xiqiu Han [a,b], Yejian Wang [a], Zhongyan Qiu [a], Tong Zong [c], Jiqiang Liu [a], Honglin Li [a], Xucheng Xu [a]

[a] Key Laboratory of Submarine Geosciences & Second Institute of Oceanography, Ministry of Natural Resources, Hangzhou 310012, China
[b] Ocean College, Zhejiang University, Zhoushan 316021, China
[c] College of Architectural Engineering, Weifang University, Weifang 261061, China

ARTICLE INFO

Keywords:
Carlsberg Ridge
Mantle source
Lithological heterogeneity
Pyroxenite
Gondwana Supercontinent

ABSTRACT

The geochemical heterogeneity of the mantle source beneath the mid-ocean ridge has been well studied, while the lithologic variability within the source has yet been rarely mentioned. We report new major, trace elements, and Sr-Nd-Pb isotopic data of fresh mid-ocean ridge basalts from the northern part of Carlsberg Ridge (i.e., CR Seg-1). The geological and geophysical observations, such as the lesser spreading rate, greater axial depth, and higher mantle Bouguer anomaly of the Seg-1, all indicate magma deficiency and lower melting degree, whereas the segment's lower average Na_8 and higher Ca_8/Al_8 indicate a higher apparent melting degree. These contradictions cannot be reconciled by melting the lithologically homogeneous peridotite mantle. We proposed that fusible pyroxenite components in the Seg-1 source melt preferentially and generate lower Na_8 magma. Moreover, it cools the ascending mantle and decreases the supply of melt derived from peridotite, leading to a magma shortage in the segment. The garnet signature revealed by the rare earth elements, higher Zn/Fe and Fe/Mn ratios, and source enrichment evidenced by Sr-Nd-Pb isotopes, support the presence of a trace quantity of garnet-pyroxenite in the mantle source. The mixing model of trace elements supports the origin of Seg-1 MORBs by mixing the depleted peridotite-derived melt and the enriched pyroxenite-derived melt. Based on the significant negative correlation between Fe/Mn and $^{206}Pb/^{204}Pb$, the delaminated lower continental crust, which might not be completely homogenized in the convective mantle, may have been transformed into the pyroxene-rich rock. The retained material would then result in lithological heterogeneity, probably in the form of pyroxenite, and cause geochemical anomalies within the source mantle for mid-ocean ridge basalts.

1. Introduction

Before the eruption, the mid-ocean ridge basalt (MORB), generated by decompression melting of the upper mantle, goes through a complicated series of magmatic evolutions, such as magma mixing and fractional crystallization, which results in its geochemical differences (Coogan and O'Hara, 2015; Niu, 2021). Moreover, the mantle source, whose heterogeneity is widespread in the upper mantle, controls the MORB composition (Hofmann, 2004; Meyzen et al., 2007; White, 2015). Both geochemical and lithological observations of the mantle's heterogeneity can be made, although the latter has mostly been ignored (Liu et al., 2008; Stracke and Bernard, 2008). Although Matzen et al. (2017) proposed that melts from metasomatic pyroxenites are not required for oceanic basalts, multiple studies emphasize that the ratio of pyroxenites to peridotites in the mantle source under the mid-ocean ridges primarily controls the composition of basalts (Russo et al., 2009; Zhang et al., 2012; Brunelli et al., 2018). The widely distributed pyroxenite/eclogite veins observed in mantle xenoliths and ultramafic massifs also support the lithological mantle heterogeneity (Lambart et al., 2013, 2016; Warren et al., 2009).

The distinct geochemical properties of the Indian Ocean mantle may be attributed to the following: (1)subducted ancient recycled oceanic crust or sediments (Rehkämper and Hofmann, 1997; Wang and Zhang, 2022); (2) recycled metasomatized oceanic lithosphere during Gondwana assembly (Saha et al., 2020); (3) delaminated lower continental crust related to Gondwana break-up (Escrig et al., 2004; Meyzen et al.,

* Corresponding author at: Key Laboratory of Submarine Geosciences & Second Institute of Oceanography, Ministry of Natural Resources, Hangzhou 310012, China.
E-mail address: yuxing@sio.org.cn (X. Yu).

https://doi.org/10.1016/j.lithos.2022.106980
Received 14 June 2022; Received in revised form 30 November 2022; Accepted 30 November 2022
Available online 5 December 2022

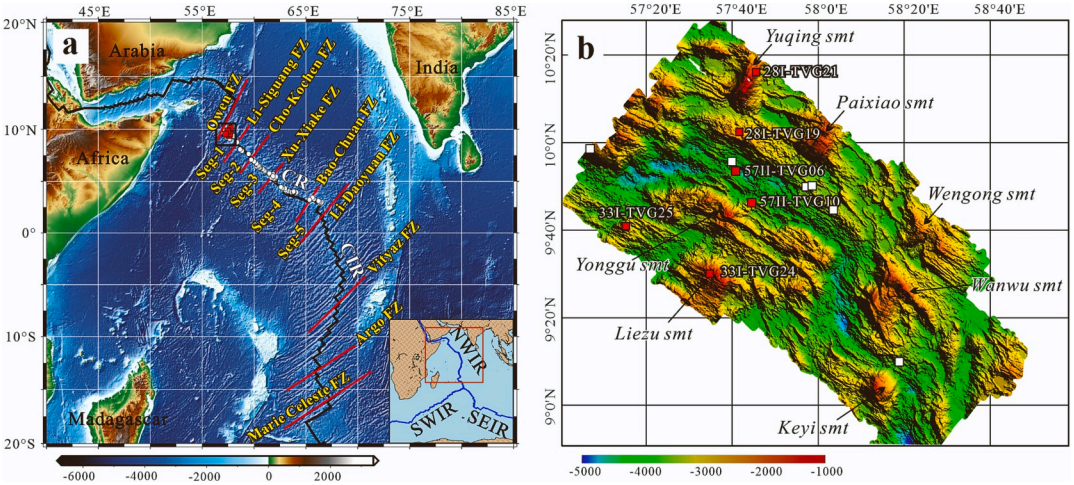

Fig. 1. Bathymetric map showing the Indian Ocean ridge system. The locations of newly collected samples are shown in red squares, while those from the literature are in white. (For interpretation of the references to colour in this figure legend, the reader is referred to the web version of this article.)

2005; Sato et al., 2022); and (4) delamination and recycling of ancient continental lithosphere during the closure of Mozambique ocean (Hanan et al., 2004; Saha et al., 2021; Falloon et al., 2022). Moreover, these processes of mantle source modification may introduce pyroxene-rich lithologies into the peridotitic mantle (Lambart et al., 2016).

Since two decades ago, it has been suggested that the mantle beneath the Indian Ocean contains lithologic heterogeneity (Salters and Dick, 2002). Pyroxenite has been dredged at the Southwest Indian Ridge (SWIR) and interpreted by melting crystallization (Warren et al., 2009). However, Brunelli et al. (2018) claimed that pyroxenite was present in the SWIR mantle. The Southeast Indian Ridge (SEIR) mantle's lithological heterogeneity and the presence of a small percentage of fusible pyroxenite within the source were suggested by Russo et al. (2009) and Graham et al. (2014).

Carlsberg Ridge (CR), part of the Northwest Indian Ocean (NWIR), shows significant geochemical variations along the ridge axis (Yu et al., 2019). Ray et al. (2013) and Chen et al. (2017) have proposed that the geochemistry of the CR basalt reflects mantle heterogeneity, which was contaminated by both recycled upper and lower continental components. However, the presence of pyroxenites in the CR mantle has not been well constrained. In this study, we reported new geochemical data of MORBs from the northern part of CR (Seg-1) and analyzed the along-axis chemical variations. Combined with the geological background, we proposed that the lithological composition of the CR mantle may be heterogeneous at the segment scale, and the existence of a pyroxene-rich component characterizes the mantle source.

2. Geological backgrounds

The break-up of the Gondwana supercontinent and the subsequent spreading of SWIR, SEIR, and NWIR have shaped the current Indian Ocean, characterized by three spreading branches converging at the

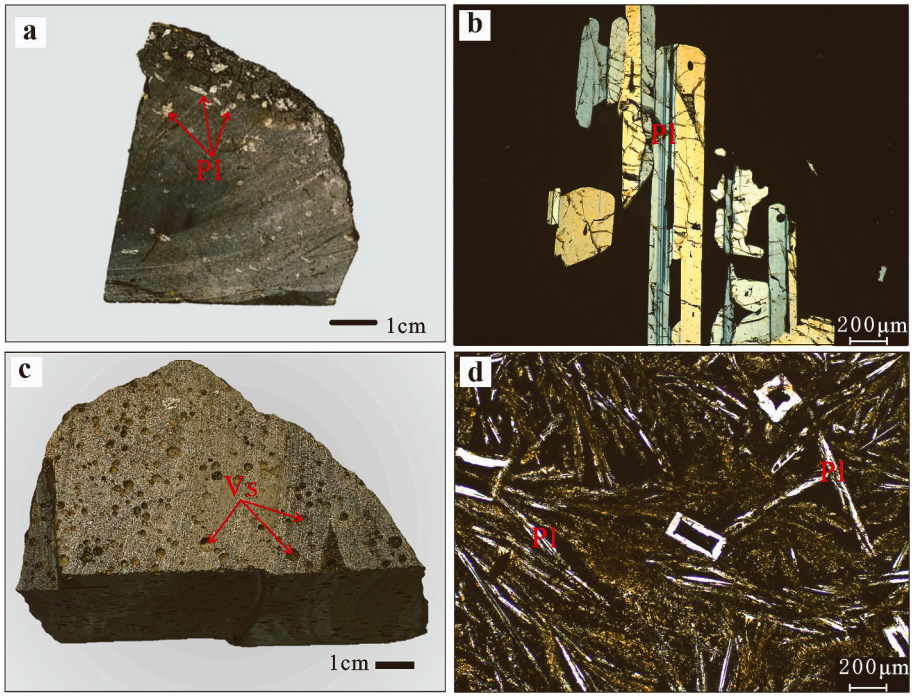

Fig. 2. Hand specimens and photomicrographs of typical basalts from CR Seg-1. (a) and (b) Basalt with large plagioclase phenocrysts (33I-TVG25), (c) and (d) Basalt with abundant vesicles (28I-TVG21). More photomicrographs can be found in Fig. S1.

Table 1
Representative major (wt%) and trace element (ppm) compositions of basalts from CR Seg-1.

Sample	28I-TVG19	28I-TVG21	33I-TVG 24–1	33I-TVG 24–2	33I-TVG 24–3	33I-TVG 25–1	33I-TVG 25–2	33I-TVG 25–3	57II-TVG06	57II-TVG10
Long.(°E)	57.67	57.73	57.55	57.55	57.55	57.24	57.24	57.24	57.66	57.71
Lat.(°N)	10.02	10.24	9.52	9.52	9.52	9.68	9.68	9.68	9.88	9.76
Material	WR	WR	WR	WR	WR	WR	WR	WR	WR	Glass
SiO_2	*50.4**	*50.2*	49.76	*49.77*	49.97	*50.12*	50.13	50.26	51.0	20.29
TiO_2	*1.78*	*1.98*	1.83	*1.87*	1.84	*1.53*	1.52	1.54	1.39	0.86
Al_2O_3	*14.95*	*15.1*	15.42	*15.83*	15.6	*16.4*	16.2	15.99	15.48	15.98
FeOt	*10.86*	*11.43*	11.33	*11.28*	11.31	*10.28*	10.21	10.33	8.55	7.75
MnO	*0.16*	*0.17*	0.18	*0.19*	0.18	*0.17*	0.17	0.17	0.15	0.15
MgO	*7.89*	*6.07*	6.76	*6.36*	6.61	*6.65*	6.83	7.03	8.9	10.63
CaO	*10.35*	*10.15*	10.25	*10.5*	10.35	*10.8*	10.8	10.8	10.71	12.07
Na_2O	*2.98*	*3.46*	3.1	*3.18*	3.13	*3.27*	3.24	3.22	2.91	1.89
K_2O	*0.27*	*0.27*	0.23	*0.26*	0.26	*0.23*	0.28	0.32	0.17	0.04
P_2O_5	*0.2*	*0.21*	0.21	*0.24*	0.22	*0.16*	0.16	0.16	0.14	0.06
Total	*99.84*	*99.04*	99.07	*99.48*	99.47	*99.61*	99.54	99.82	99.37	99.71
Mg#	*56.42*	*48.63*	53.55	*54.39*	54.81	*51.54*	50.12	51.02	64.98	70.95
K/Ti	*0.15*	*0.14*	0.13	*0.14*	0.14	*0.15*	0.18	0.21	0.17	0.06
Sc	*37.7*	*38.8*	37	*36*	34.9	*33.3*	35	35.8	34.9	33.2
V	*274*	*282*	305	*320*	305	*277*	260	275	251	227
Cr	*241*	*129*	192	*185*	193	*200*	207	208	363	540
Co	*45.3*	*44*	40.8	*40*	39.9	*37*	38.8	39	58.3	57.0
Ni	*140*	*81.7*	104.5	*96.8*	102.5	*72.2*	77.9	83.1	181	269
Cu	*53.6*	*53.1*	54.4	*53.9*	51.4	*56.5*	61.6	63	57.2	71.4
Zn	*90*	*99*	96	*98*	91	*86*	81	79	70.3	64.9
Ga	*18.4*	*19.65*	19.45	*19.55*	19.7	*17.65*	18.55	18.35	15.4	14.1
Ge	*0.17*	*0.2*	0.19	*0.3*	0.22	*0.32*	0.24	0.2	–	–
Rb	*3.1*	*4.1*	2.1	*2*	1.8	*1.5*	2	2.6	1.3	0.43
Sr	*132*	*165*	152.5	*164.5*	154.5	*167*	164.5	161	148	64.9
Y	*41.5*	*45.1*	42.9	*42.6*	42.8	*34.1*	34.9	35.5	31.6	23.4
Zr	*142*	*164*	162.5	*160*	160.5	*124*	128.5	130.5	101	41.9
Nb	*3.6*	*2.9*	3.3	*3.5*	3.2	*2.2*	2	2.2	2.53	0.86
Cs	*0.16*	*0.19*	0.06	*0.04*	0.04	*0.05*	0.05	0.11	0.01	0.01
Ba	*16.5*	*15.8*	18.9	*18.6*	19	*11.5*	11.7	9.1	13.9	3.95
Hf	*3.6*	*4*	4.3	*4.3*	4.2	*3.3*	3.4	3.5	2.51	1.28
Ta	*0.25*	*0.22*	0.21	*0.22*	0.2	*0.15*	0.15	0.15	0.19	0.15
Pb	*0.9*	*1.3*	0.7	*0.9*	0.8	*0.6*	0.7	0.6	0.61	0.24
Th	*0.29*	*0.22*	0.25	*0.25*	0.25	*0.15*	0.15	0.16	0.17	0.06
U	*0.17*	*0.18*	0.1	*0.13*	0.12	*0.09*	0.08	0.12	0.09	0.02
La	*5.5*	*7*	5.6	*6*	5.7	*4.9*	4.4	4.6	3.74	1.26
Ce	*17.8*	*21.4*	18	*17.25*	17.95	*13.75*	14.25	14.55	11.7	4.15
Pr	*2.46*	*3.07*	2.71	*2.77*	2.67	*2.24*	2.37	2.23	1.9	0.77
Nd	*14.9*	*16.8*	14.6	*15.1*	14.6	*12.1*	12.8	11.9	10.5	4.6
Sm	*4.68*	*5.34*	4.91	*5.04*	4.76	*4.09*	4.31	4	3.58	1.92
Eu	*1.58*	*1.69*	1.6	*1.69*	1.61	*1.41*	1.47	1.35	1.26	0.79
Gd	*6.35*	*7.04*	6.82	*7.01*	6.69	*5.61*	5.59	5.55	4.41	2.88
Tb	*1.07*	*1.19*	1.16	*1.15*	1.15	*0.97*	0.99	0.96	0.82	0.54
Dy	*7.44*	*7.81*	7.16	*7.13*	7.25	*5.93*	5.8	5.95	5.42	3.76
Ho	*1.58*	*1.72*	1.49	*1.54*	1.5	*1.25*	1.25	1.25	1.17	0.82
Er	*4.65*	*4.82*	4.4	*4.58*	4.49	*3.8*	3.71	3.73	3.31	2.34
Tm	*0.66*	*0.68*	0.64	*0.67*	0.65	*0.56*	0.6	0.55	0.49	0.35
Yb	*4.17*	*4.54*	3.99	*3.97*	3.96	*3.2*	3.47	3.39	3.05	2.22
Lu	*0.65*	*0.66*	0.59	*0.61*	0.6	*0.49*	0.5	0.51	0.46	0.33

Rodriguez Triple Junction (Chatterjee et al., 2013). The northwest branch of NWIR consists of the Carlsberg Ridge (CR) and Central Indian Ridge (CIR), separated by the Li-Daoyuan fracture zone (FZ) (Yu et al., 2019). The complete spreading rate increases from 22 mm/yr at the northern end of the CR close to Owen FZ to nearly 46 mm/yr at the southern tip of the CIR close to the Rodrigues Triple Junction (Murton and Rona, 2015).

The Carlsberg Ridge, extending from 2°N-10°N, is a typical slow-spreading mid-ocean ridge that spreads at a total rate of 24–26 mm/yr. It formed in Cenozoic while the microcontinent Seychelles bank has been separated from the Indian block since 65 Ma (Collier et al., 2008; Yu et al., 2019). There are five ridge segments, divided by four major transform faults: the Li-Siguang FZ, Cho-Kochen FZ, Xu-Xiake FZ, and Bao-Chuan FZ from north to south (Fig. 1). The segment at the northern end (Seg-1) extends ~250 km from northwest to southeast between 57°E-58.5°E with zigzagged ridge axis (Han et al., 2012; Yu et al., 2019). As the oceanic crust increasingly thickens to the southeast and the supply of magma increases, the mantle Bouguer anomaly and axial depth gradually decrease from Seg-1 to Seg-5, indicating a relative magma shortfall for Seg-1 (Han et al., 2012; Murton and Rona, 2015). Moreover, high-relief non-conical seamounts, recognized as oceanic core complexes with corrugated surfaces, are widely distributed on the Seg-1 ridge flanks, indicating the inadequacy of magma supply (Han et al., 2012).

3. Results

3.1. Petrographic characteristics

Six TV-grab stations of basaltic samples were collected from CR Seg-1 during the cruises DY28, DY33, and DY57 (Fig. 1). All samples collected were dark grayish to black dense massive basalts, some of which had been coated with millimeter-thick ferromanganese crust. Clusters of large plagioclase phenocrysts or millimeter-sized vesicles could be observed in some hand specimens (Fig. 2). In the outer layer of the rock, where they quenched more rapidly, the plagioclase phenocryst with

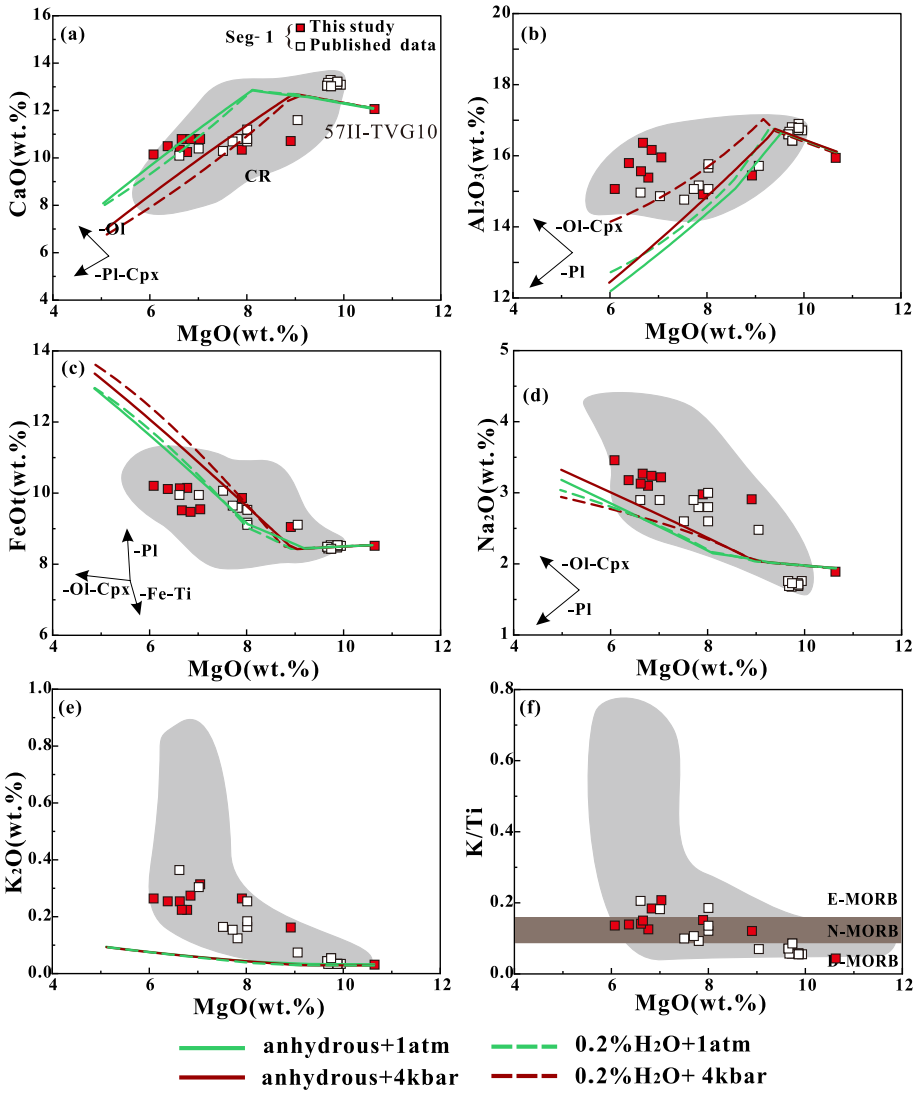

Fig. 3. Correlations of major elements (a) FeOt, (b) Al_2O_3, (c) K_2O, (d) Na_2O, (e) K/Ti, and (f) CaO with MgO for Seg-1 basalt samples. Published data from Melson et al. (2003), Murton and Rona (2015), and Arevalo and McDonough (2008). The gray field represents CR MORBs, and the data are from PetDB. The liquid line of descent (LLD) was calculated using Petrology3 (Danyushevsky and Plechov, 2011). Sample 57II-TVG10 was chosen as the primary melt. Both mineral-melt equilibrium models under anhydrous and 0.2% H_2O conditions were carried out at a pressure of 1 atm and 4 kbar, respectively, following Weaver and Langmuir (1990), Ariskin et al. (1993), and Danyushevsky (2001).

shining crystal faces are more common, and the crystals were sustained in glassy groundmass as a vitrophyric texture (Fig. 2a, b). Some samples occurred with vesicles, whereas most vesicular specimens can retain up to 5% of their vesicles (Fig. 2c). Under the microscope, the plagioclase phenocrysts with a euhedral crystal lath shape can be observed in a glomeroporphyritic texture. Most plagioclases are easily distinguished by their twin crystals, and some have clear resorption pitted structures, that demonstrate how the initial plagioclase and the later-formed magma interacted. The glassy matrix can be devitrified into the microcrystals of fibrous plagioclase and small pyroxene, thus forming a variolitic texture (Fig. 2d).

3.2. Major elements geochemistry

Ten fresh samples from six stations were analyzed for their major and trace elements, at ALS Chemex (Guangzhou) Co., Ltd., China. The new major and trace elements are listed in Table 1. Seg-1 basalts have total alkalis ($Na_2O + K_2O$) concentration between 1.72 and 3.73 wt%, with SiO_2 of 49.76–51.7 wt%, indicating compositions typical of tholeiite in TAS and AFM diagrams (Fig. S2). The MgO varied from 6.07 to 10.63 wt %, with Mg# of 51–71. The Na_2O, K_2O, and FeOt contents decreased, but the CaO and Al_2O_3 increased as MgO increased (Fig. 3). The Seg-1 samples have K/Ti values of 0.04–0.21, extending from D-MORB to *E*-MORB, classified as K/Ti < 0.09 and K/Ti > 0.15, respectively (Gale et al., 2013; Standish et al., 2008). Compared to the remaining samples from Seg-1, the basaltic glasses' published data by Melson et al. (2003) demonstrate higher Al_2O_3 and CaO and lower TiO_2, FeOt, Na_2O, and K_2O contents. The off-axis basaltic samples (e.g., 28I-TVG21,33I-TVG24 and 33I-TVG25) have relatively lower MgO content, and higher Al_2O_3 at a given MgO than the rest (Fig. 3). The major element contents of Seg-1 are comparable with the rest of the CR segments.

3.3. Trace element geochemistry

The samples from Seg-1 have La/Sm_N ratios that are considerably lower (0.42–0.85) and moderate Th/La ratios of (0.031–0.053) that are more characteristic of N-MORB or even D-MORB (Fig. 4a and b). The chondrite-normalized rare earth elements (REE) show similar patterns, all depleted in light REEs, with negative Eu, and Sr anomalies (Fig. 4c and d). Seg-1 basalts and D-MORB are comparable, as shown by the primitive mantle-normalized incompatible trace element diagram (Fig. 4d). The trace element compositions of Seg-1 are all within the range of the rest of the CR, except 57II-TVG10. The sample 57II-TVG10 has a uniquely lower content of REEs, with the lowest La/Sm_N ratio, and no negative Eu anomaly.

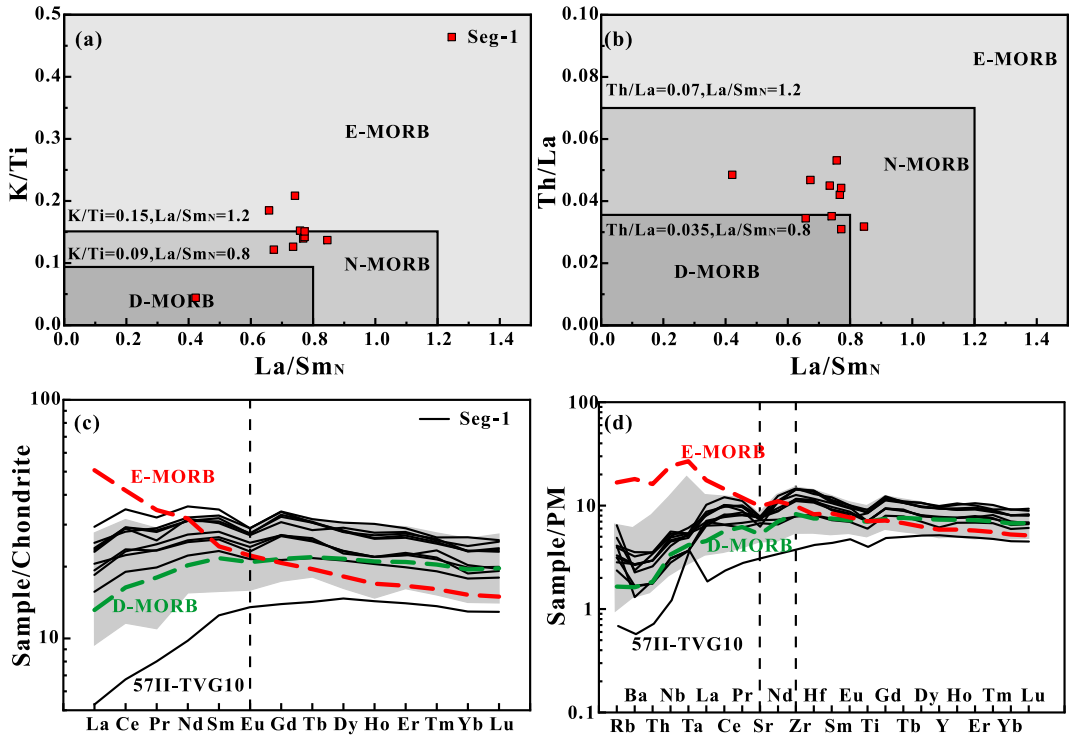

Fig. 4. (a)K/Ti versus La/Sm_N, (b) Th/La versus La/Sm_N, (c) Chondrite-normalized REE diagram, (d) primitive mantle-normalized multi-element spider diagram of Seg-1 basalts. The shaded areas in Fig. 4c and d represent the trace element compositions of the full Carlsberg Ridge. The compositions of chondrite and primitive mantle are from Sun and McDonough (1989). D-MORB and *E*-MORB are from Gale et al. (2013).

Table 2
Sr-Nd-Pb isotopic compositions of basalts from CR Seg-1.

Sample	$^{87}Sr/^{86}Sr$	2SE	$^{143}Nd/^{144}Nd$	2SE	$^{206}Pb/^{204}Pb$	2SE	$^{207}Pb/^{204}Pb$	2SE	$^{208}Pb/^{204}Pb$	2SE
28I-TVG19	0.702945	(±7)	0.513137	(±10)	17.707	(0.0007)	15.469	(0.0006)	37.619	(0.0016)
	0.702697[#]		*0.513133*		*17.528*		*15.412*		*37.33*	
28I-TVG21	0.703329	(±6)	0.513132	(±10)	17.824	(0.0011)	15.484	(0.0009)	37.747	(0.0023)
	0.702772		*0.51315*		*17.593*		*15.415*		*37.392*	
33I-TVG24–1	*0.702635*		*0.513122*		*17.586*		*15.402*		*37.312*	
33I-TVG24–2	0.702984	(±8)	0.513143	(±6)	17.709	(0.0014)	15.427	(0.0012)	37.411	(0.0034)
33I-TVG25–1	*0.702689*		*0.513105*		*17.567*		*15.416*		*37.342*	
33I-TVG25–2	0.702909	(±12)	0.513123	(±10)	17.731	(0.0014)	15.452	(0.0012)	37.52	(0.0028)
57II-TVG06	0.702694	(±14)	0.513129	(±10)						
57II-TVG10	0.702698	(±10)	0.513131	(±18)						

[#] Those data of isotopes in italic are analyzed in WHOI, otherwise from the State Key Laboratory for Mineral Deposits Research, Nanjing University.

3.4. Sr-Nd-Pb isotopes

Eight samples were selected to perform the Sr-Nd-Pb isotopic analysis. Among them, four were measured using MC-ICP-MS on the Thermo-Finnigan Neptune at the Woods Hole Oceanographic Institute. The rest were analyzed at the State Key Laboratory for Mineral Deposits Research, Nanjing University with a Finnigan Triton TI thermal ionization mass spectrometer and a Neptune Plus MC-ICP-MS. The new isotopic data are listed in Table 2. The $^{87}Sr/^{86}Sr$ and $^{143}Nd/^{144}Nd$ varied from 0.70263 to 0.70333 and 0.51311–0.51314 for Seg-1, respectively (Fig. 5a). While the Sr isotope ratios are slightly erratic, the Nd isotopic ratios are relatively constant. The Pb isotopic ratios of Seg-1 are lower than those of the rest NWIR basalts, with $^{206}Pb/^{204}Pb$ of 17.59–17.82, $^{207}Pb/^{204}Pb$ of 15.40–15.48, and $^{208}Pb/^{204}Pb$ of 37.31–37.75, which signifies the long-term low U/Pb and Th/Pb ratios for the mantle source. All the Seg-1 samples are plotted above the Northern Hemisphere Reference Line (NHRL). In the $^{207}Pb/^{204}Pb$ vs. $^{206}Pb/^{204}Pb$ plot, all the samples show deviate from DM to EMI and lower continental crust (LCC) (Fig. 5c and d).

4. Discussion

4.1. Magmatic evolution of Seg-1 basalts

4.1.1. Effects of seawater alteration

Fresh basalt chips or glasses were selected for major and trace element analysis, to avoid seawater alteration. The Loss on ignition (LOI) of the Seg-1 samples ranged from −0.79 to 0.61(<1 wt%), signifying negligible alterations, as a higher degree of rock alteration might be expected to have elevated LOI. Our samples were discriminated based on an alteration box plot from Large et al. (2001). Consequently, almost all samples are within the field of the least altered box (Fig. S3).

The concentration of fluid-mobile elements (K, U, and La) will increase in altered basalt layers while the fluid-immobile elements (Nb) remain constant (Michard and Albarede, 1985). Furthermore, the relatively constant K_2O/Rb and K_2O/Nb ratios of the Seg-1 samples imply limited alteration. Therefore, it is possible to conclude that the impact of seawater alteration was ignorable for the study samples when paired with petrographic features under a microscope.

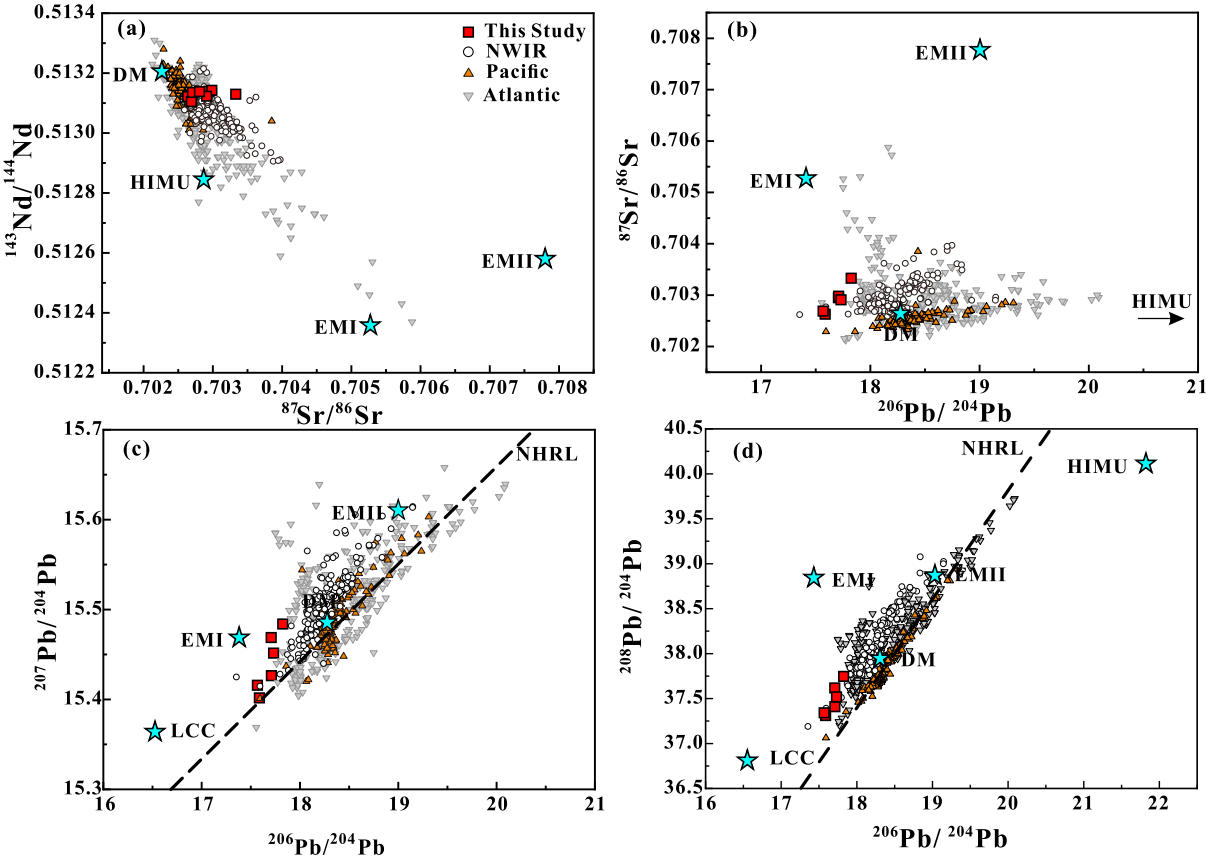

Fig. 5. Sr-Nd-Pb isotope diagrams for basalts from Seg-1. The data for the NWIR, Pacific and Atlantic mid-ocean ridges are from PetDB. The end member's data sources are: DM from Workman and Hart, 2005; HIMU, EMI, and EMII from Armienti and Gasperini (2007); LCC from Escrig et al. (2004).

4.1.2. Fractional crystallization

The FeOt, Na_2O, K_2O, Al_2O_3, and CaO versus MgO correlations indicate extensive crystallization differentiation (Fig. 3). The Ni and Cr elements are compatible with olivine and clinopyroxene (Rollinson, 1993). Therefore, the crystallization of olivine and/or clinopyroxene will decrease the content of MgO, Ni, and Cr. The Ni and Cr variations along with MgO and Y of Seg-1 basalts indicate the crystallization of olivine and clinopyroxene (Fig. S4). Plagioclase is usually enriched in Sr and Eu; thus, the fractionation of plagioclase will decrease the contents of Sr and Eu. The Sr content decreased with increasing Y, indicating the fractionation of plagioclase, consistent with the slightly negative Eu anomaly, as well as the phenocrysts observed under a microscope. The abundance of REE in Seg-1 samples is generally higher than that of D-MORB, and parallel to each other, due to the mineral crystallization.

Sample 57II-TVG10 is basaltic glass, other than whole rocks. The glass is less fractionated, therefore, higher in MgO and lower in REE content than the other samples (Figs. 3 and 4). Besides, it was collected from the ridge axis and represents the newest magma from the ridge. The mantle source for the 57II-TVG10 could be more depleted than the earlier-formed off-axis samples (e.g. 28I-TVG19), thus showing lower La/Sm.

Quantitative modeling of the fractional crystallization for Seg-1basalts has been performed using Petrolog3 software, selecting sample 57II-TVG10 as the primary melt (Fig. 3). The fractional crystallization was modeled at different pressures (1 atm, 4 kbar) with different H_2O contents. The liquid lines of descent (LLDs) under different pressures are parallel, while the one at 4 kbar under anhydrous conditions passes through most of the Seg-1 samples. Plagioclase crystallization can be significantly inhibited with the presence of water (Asimow and Langmuir, 2003), which causes LLD to change to a higher Al_2O_3 state (Fig. 3b). Moreover, the magma differentiation under high pressures will favor the crystallization of clinopyroxene before plagioclase, thus resulting in higher Al_2O_3 of the magma (Eason and Sinton, 2006). High pressure or hydrous differentiation could form the abnormally high Al content for some Seg-1 basalts. The major element compositions of the basalt glass from Melson et al. (2003) deviate from the simulated LLD, which indicates that the single-parent magma cannot explain the compositional differences in Seg-1 basalts.

4.1.3. Mantle melting process

In addition to the later seawater modification and crystallization differentiation, the mantle source composition and the degree of melting affect the compositional variety of MORBs. Na_8 and Ca_8/Al_8 can be used to calculate the melting degree of the mantle source (Gale et al., 2014; Klein and Langmuir, 1987). However, Na_8 is defined as a homogeneous mantle, and the degree of melting calculated from Na_8 might not always represent the actual melting characteristics of the mantle (Klein and Langmuir, 1987; Salters and Dick, 2002). Compared to the melting degree calculated by relic minerals in mantle peridotite, the result calculated through basalt is defined as the apparent melting degree (Brunelli et al., 2018). Obvious contrast of Na_8 (1.88–3.04) and Ca_8/Al_8 (0.63–0.80) can be observed among the samples from Seg-1, which implies two distinct groups of melts (Fig. 6a). According to Plank and Langmuir's (1992) algorithm, the apparent melting degree for Seg-1 ranging from 16% to 28%. The contribution of melts with different melting degrees in Seg-1 is also supported by trace element variation diagrams. Seg-1 samples exhibit positive correlations between La/Sm_N and La, Zr/Y and Zr, Zr/Y, and La/Sm_N (Fig. 6b, d).

4.2. Distinct geochemical and geophysical features of Seg-1

Systematic variations in major elements were reported for the basalts

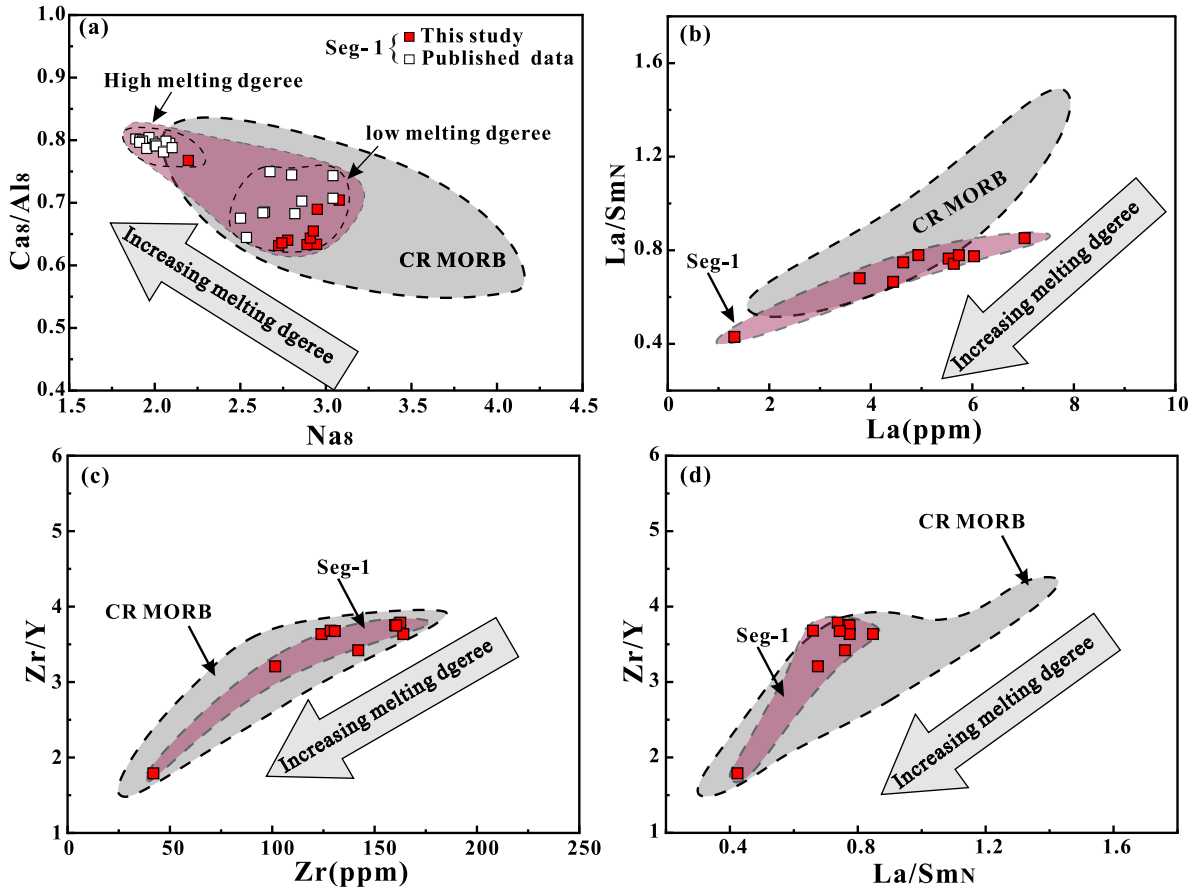

Fig. 6. (a) Ca_8/Al_8 vs. Na_8 (b) La vs $(La/Sm)_N$, (c) Zr vs Zr/Y and (d) $T(La/Sm)_N$ vs.Zr/Y. for Seg-1 basalts.

from CR (Fig. 7). Basalts' gradually rising Na_8 content from north to south, indicates that Seg-1 has a higher apparent melting degree, which is consistent with the statistical findings reported by Murton and Rona (2015). The average apparent melting degree of Seg-1 is 21.0% and gradually decreases southward to 17.9% at Seg-5, which implies that the Seg-1 should have more magma supply and thicker oceanic crust than the rest ridge segments if the mantle source is homogeneous along the ridge axis.

However, the actual geophysical observations show deeper axial depth and higher mantle Bouguer anomaly for Seg-1 (Cannat et al., 2008; Han et al., 2012), which indicates a relatively thinner crust and lower melt supply of Seg-1. The actual smaller melt supply contradicts the higher apparent melting degree of Seg-1. This contradiction argues against a homogeneous peridotite mantle source. Therefore, there might be a few pyroxenite components in the mantle of Seg-1, which has a lower solidus temperature than that of peridotite. Additionally, Seg-1 basalts have the lowest $^{206}Pb/^{204}Pb$ ratios among all CR segments (Fig. 7f), also implying the unique mantle source composition under Seg-1.

Pyroxenite-derived melts with a high melting degree have lower Na_8 and higher Ca_8/Al_8 (Lambart et al., 2013), resulting in a higher apparent melting degree. Besides, the prior melting of pyroxenite will cause mantle undercooling by subtraction of latent heat, which in turn limits the melting of peridotite (Phipps, 2001; Brunelli et al., 2018). The higher apparent melting degree does not follow with abundant magma supply, thus resulting in thin a crust and a higher Bouguer anomaly.

4.3. *Lithological heterogeneity of the mantle source*

In addition to a straightforward peridotitic mantle source, oceanic basalt's varied isotopic and trace element compositions may reflect the lithological heterogeneity (Stracke and Bernard, 2008; Zhang et al., 2012). The lithologic heterogeneity of the mantle may exist in the form of pyroxenite dispersed in the host peridotite mantle. Pyroxene-rich rocks are common in mantle xenoliths, orogenic massifs, and ophiolites, permitting a fair assumption for their occurrence even when there is no direct evidence for it (Lambart et al., 2009, 2013). The solidus temperature of pyroxenite is lower than that of peridotite, therefore, the melting degree of pyroxenite is generally higher than that of peridotite. Pyroxenite only forms a small percentage of the mantle (Lambart et al., 2016), yet its melt still contributes significantly to MORB (Hirschmann and Stolper, 1996; Sobolev et al., 2007). The decoupling of melting degrees calculated by mantle peridotites and associated MORBs shows that pyroxenites are widely distributed in sub-ridge mantle sources (Brunelli et al., 2018). The geochemical and geophysical features indicate lithological heterogeneities in the mantle source of CR Seg-1.

The REE compositions show that Seg-1 basalts have relatively higher Sm/Yb_N, indicating a stronger garnet signature of Seg-1 basalts than the rest of CR segments (Fig. 7e). The garnet-bearing lithologies could exist as garnet-pyroxenite and garnet-peridotite (Salters and Hart, 1989; Shen and Forsyth, 1995). If melting begins at garnet peridotite field, which means melting begins at greater depth, it would produce more magma and result in a thicker oceanic crust (Hirschmann and Stolper, 1996). This is contradicted by the actual thinner crust for Seg-1. Therefore, it favors the involvement of garnet-pyroxenite within the mantle source.

Pyroxenite represents the mafic and ultramafic pyroxene-rich plutonic rocks with <40% olivine, and its major element compositions span a wide range (Lambart et al., 2016). Because calcium is compatible with clinopyroxene but significantly incompatible with olivine, the melt from the pyroxenite source has lower CaO content than that produced by peridotite (Herzberg and Asimow, 2008; Pertermann and Hirschmann, 2003). Seg-1 MORBs are within the field of pyroxenite melts (Fig. 8a),

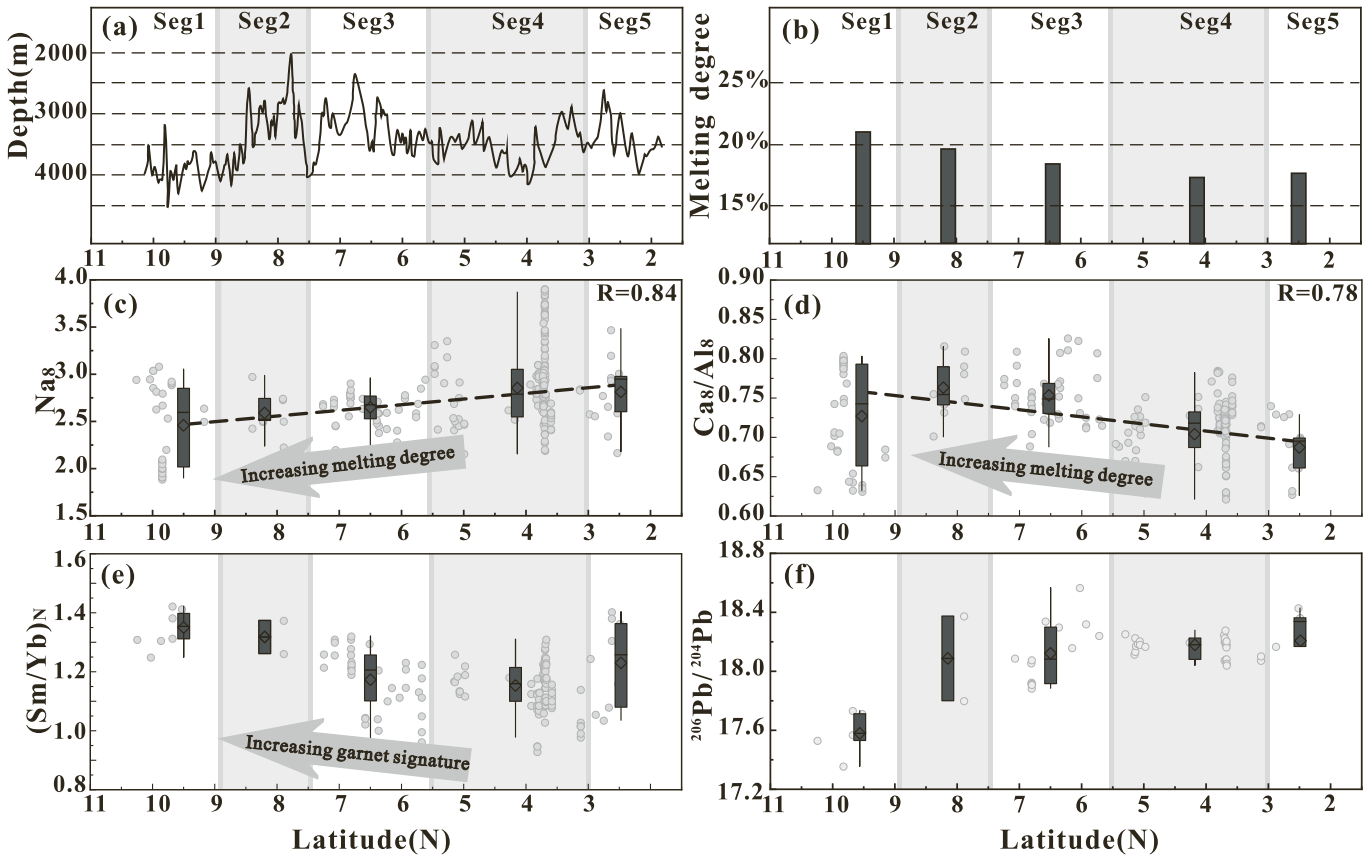

Fig. 7. Latitudinal variations along the ridge axis in the chemical composition of (c) Na_8, (d) Ca_8/Al_8, (e and f) Sm/Yb_N, and Pb isotopes. The axial depth variation (a), The average melting degrees of each segment calculated using Na_8 are shown in (b). The calculation of mantle melting degree follows Plank and Langmuir (1992). The gray circle represents the basalt data, and the green diamond represents the average value of each ridge segment. The data also included those from PetDB and Zong et al. (2020) apart from this study. (For interpretation of the references to colour in this figure legend, the reader is referred to the web version of this article.)

though the lower CaO content can also be caused by fractional crystallization.

Zn/Fe and Fe/Mn ratios are relatively stable during the fractionation of olivine and orthopyroxene but will change significantly during the fractionation of garnet and clinopyroxene (Le Roux et al., 2010, 2011). Zn/Fe and Fe/Mn ratios in garnet pyroxenite melts are higher than those in peridotite melts (Heinonen et al., 2013). Liu et al. (2008) illustrated that the Fe/Mn of anhydrous peridotite melt is <60, while the Fe/Mn of pyroxenite melt is over 60. Davis et al. (2013) demonstrated that non-peridotite-sourced basalts have Zn/Fe > 13 and Fe/Mn > 62. Le Roux et al. (2010) pointed out that the average Zn/Fe ratio in peridotites is 8.5. Seg-1 MORBs have slightly higher Zn/Fe (10.9–12.4) and Fe/Mn (53.6–61.3) than those of peridotite melts at a given MgO, which indicates the contribution of pyroxenite melts (Fig. 8b, c). Combined with the major and trace element evidence, we further propose that there is garnet-pyroxenite embedded in the mantle source of Seg-1.

4.4. Modeling of partial melting of the pyroxenite-peridotite mantle

The lithological heterogeneity changes the bulk partition coefficient of the mantle source and results in more significant variability of highly incompatible elements of the melt (Stracke and Bernard, 2008). Therefore, pyroxenite-derived melts are considered to have an important contribution to MORBs (Liang, 2020). To further constrain the contribution of pyroxenite-derived melts in MORB, the mixing of pyroxenite and peridotite-derived melts was modeled based on trace element characteristics.

DMM was selected as the depleted peridotite source, the recycled oceanic crust (ROC) and LCC as the pyroxenite source. The DMM-derived melts with a 4%–10% melting degree do not match the Seg-1 MORBs. Although, pyroxenite-derived melts under a high degree of melting (60%) have a higher abundance of trace elements (Fig. S5), the addition of 5% pyroxenite-derived melts to the D-MORBs shows an excellent match to Seg-1 MORBs (Fig. 9). Therefore, the abundance of trace elements in Seg-1 MORB can be perfectly explained by mixing DMM-derived and pyroxenite-derived melts.

The ratios of Lu/Hf and Sm/Nd are sensitive to the source's mineral composition and melting degree. Melts of pyroxenite (5%–25% melting degree) and garnet lherzolite (2%–14%) have lower Lu/Hf and Sm/Nd ratios. In comparison, the melts from depleted spinel lherzolite (2%–14%) have higher Lu/Hf and Sm/Nd ratios. The single spinel peridotite-derived melts cannot explain the Lu/Hf-Sm/Nd characteristics of Seg-1. The involvement of ROC or LCC-derived melts could better constrain the geochemical composition of Seg-1 (Fig. 10a). Pyroxenite-derived melt also had a relatively high Dy/Yb and Sm/Yb. The mixing models based on Dy/Yb-Th/Nb, Zr/Hf-Sm/Nd, Zr/Hf-Dy/Yb also support the involvement of ROC or LCC-derived melts in the magma of Seg-1 (Fig. 10b-d).

There are some outlier data in the mixing model, which can be attributed to the selected starting compositions of DMM, LCC, and ROC. Thus, the mantle source of Seg-1 is dispersed pyroxenite material in the matrix of peridotite. The addition of pyroxenite-derived melts changes the composition of erupted magma and can explain the geochemistry of Seg-1 MORBs. Although it is difficult to determine the exact proportion of involvement of pyroxenite-derived melt, our mixing model suggests that pyroxenite contributions are estimated at <5% in total.

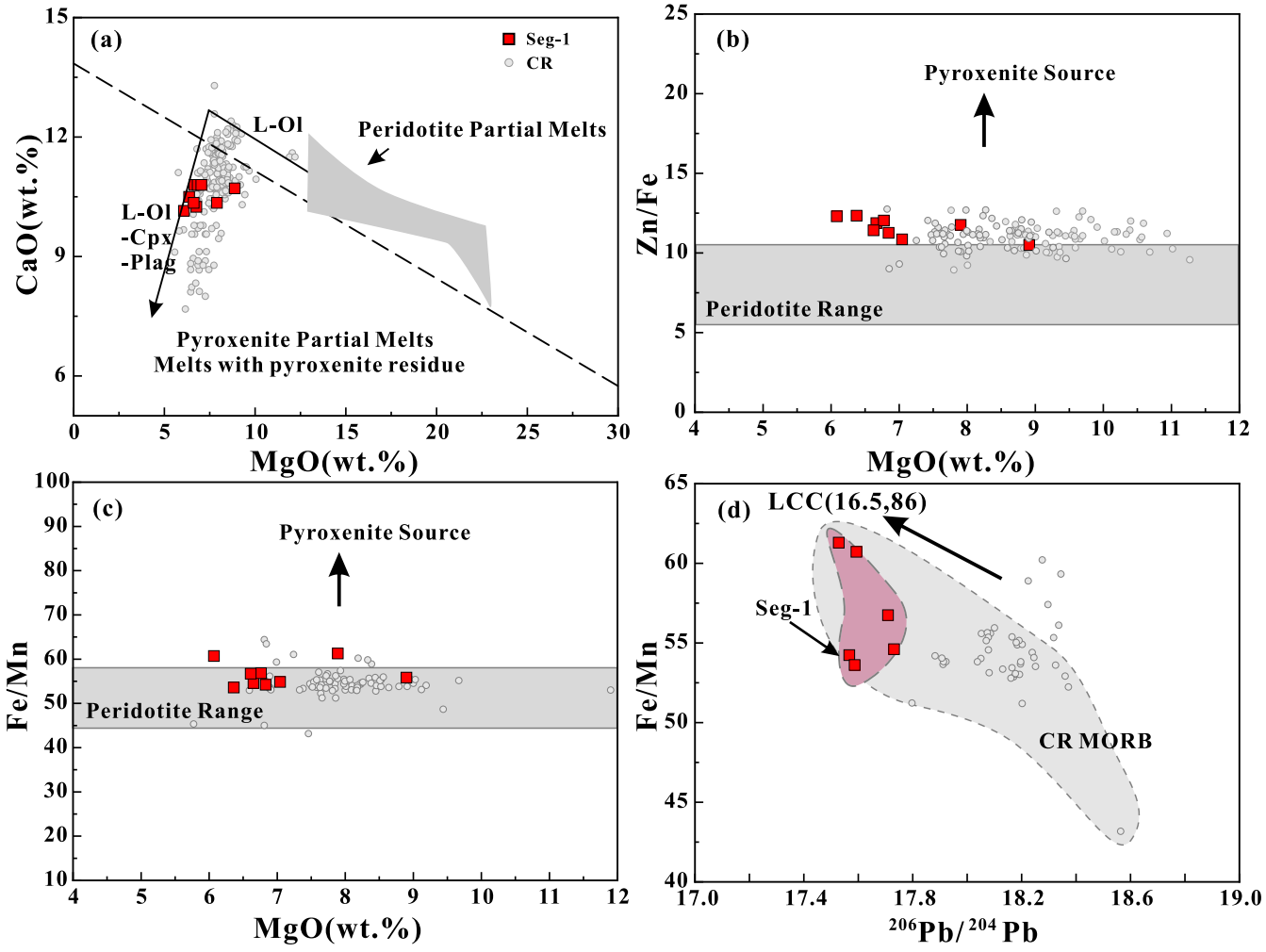

Fig. 8. Plots of bulk rock CaO (a), Zn/Fe*(10^4) (b)and Fe/Mn (c) vs. MgO for Seg-1 samples and the relationships between Fe/Mn and $^{206}Pb/^{204}Pb$ (d). The green dashed line separating pyroxenite melt from peridotite melt is based on Herzberg and Asimow (2008). The fields for Fe/Mn and Zn/Fe in the peridotite are from Liu et al. (2008) and Le Roux et al. (2011). (For interpretation of the references to colour in this figure legend, the reader is referred to the web version of this article.)

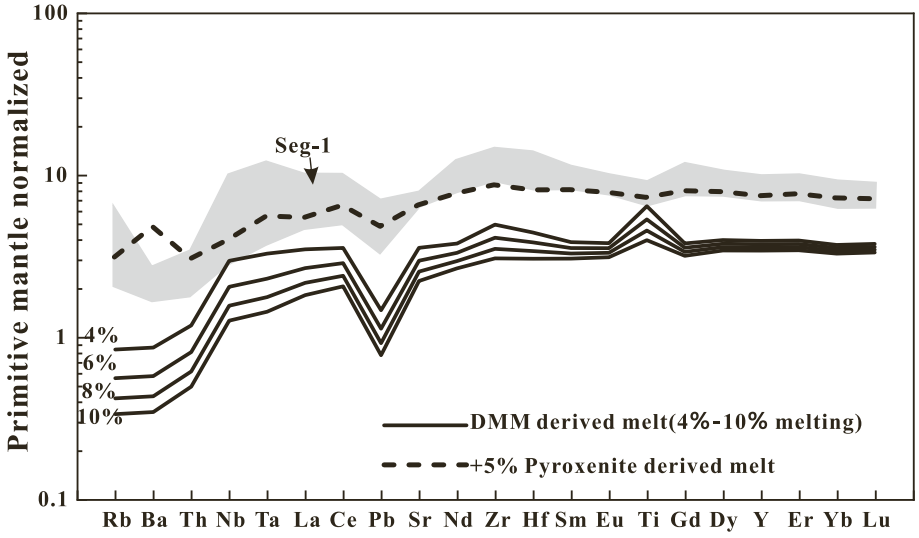

Fig. 9. Modeled trace elements for typical pyroxenite and peridotite endmembers. We calculated the melt composition with the equilibrium melting model (Shaw, 1970). The gray field represents Seg-1 MORB The partition coefficients of incompatible elements during melting are taken from experimental studies (Salters and Stracke, 2004; Krein et al., 2020). The mode composition for the pyroxenite mantle is 0.82 Cpx, 0.18 Grt (Pertermann et al., 2004), with melting mode of 0.7 Cpx, 0.3 Grt (Pertermann and Hirschmann, 2003); Depleted peridotite consist of 0.3 Cpx, 0.15 Opx, 0.53 Ol with melting mode of 1.125Cpx, −0.5 Opx, 0.375 Ol (Salters and Stracke, 2004). The trace element compositions of DMM are from Workman and Hart (2005), and PM from McDonough and Sun (1995). The composition of pyroxenite is represented by the recycled oceanic crust (ROC) and lower continental crust (LCC) (Stracke and Bernard, 2008, Rudnick and Gao, 2003).

4.5. Origin of the pyroxenite in the Seg-1 mantle

The distribution of pyroxenite in the MORB mantle source may occur more than we thought (Brunelli et al., 2018; Yang et al., 2020). It can be introduced into a mantle by subducted oceanic crust converting to pyroxene-rich rocks under mantle conditions (Zhang et al., 2012); the

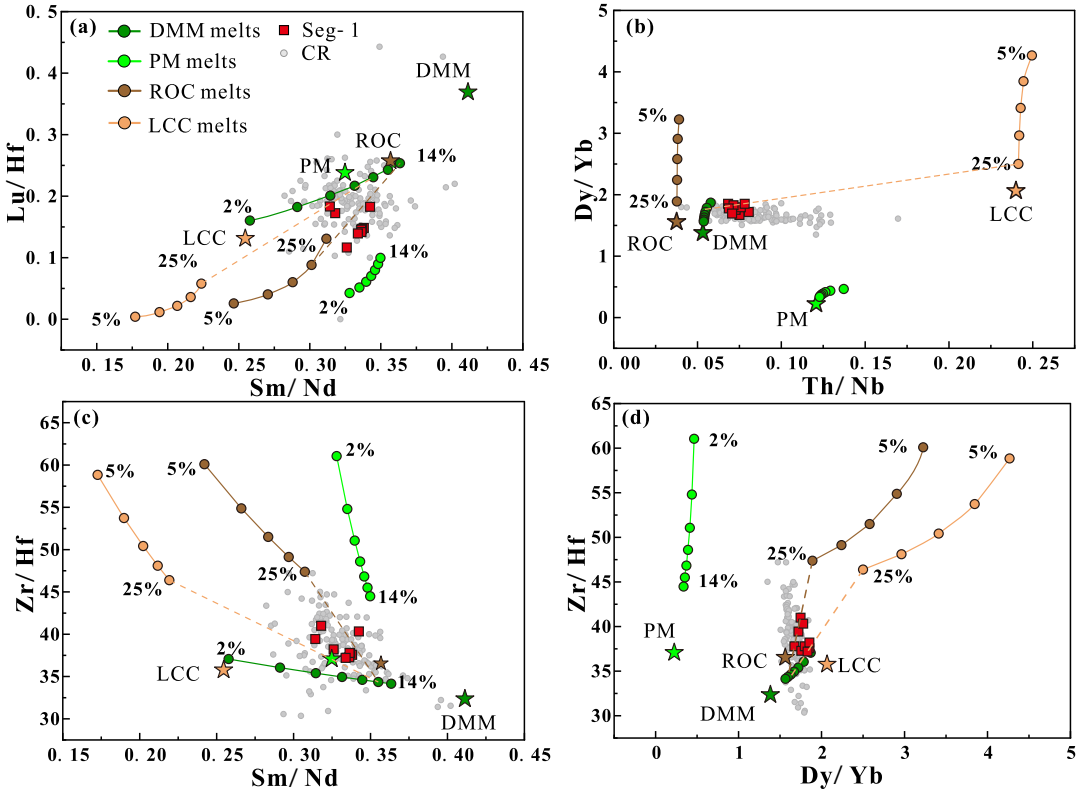

Fig. 10. Mixing models based on trace elements (a) Lu/Hf-Sm/Nd, (b) Dy/Yb-Th/Nb, (c) Zr/Hf-Sm/Nd, (d) Zr/Hf-Dy/Yb. The melting conditions are the same as described in Fig. 9.

delamination or foundering of mafic cumulates and LCC (Hirschmann and Stolper, 1996; Lee, 2014); or magma emplacement and metasomatism in the lithosphere (Humphreys and Niu, 2009; Bodinier et al., 2008).

The Indian Ocean MORBs have lower $^{143}Nd/^{144}Nd$ and higher $^{87}Sr/^{86}Sr$ as well as higher $^{207}Pb/^{204}Pb$ and $^{208}Pb/^{204}Pb$ at a given $^{206}Pb/^{204}Pb$, compared to the Pacific and Atlantic MORBs, which is so-called DUPAL anomaly (Escrig et al., 2004; Hart, 1984; Meyzen et al., 2005). Previous research has proposed many hypotheses regarding the circulation of various enriched materials into the Indian Ocean mantle, including delaminated continental crust from the cratonic Gondwana lithosphere (Zong et al., 2019; Sato et al., 2022), recycled subducted altered oceanic crust and sediment (Rehkämper and Hofmann, 1997; Wang and Zhang, 2022), and ancient recycled oceanic lithosphere (Saha et al., 2020).

The Seg-1 basalt exhibits extremely low radioactive $^{206}Pb/^{204}Pb$ and $^{207}Pb/^{204}Pb$ isotopes and shows affinity with EMI, which may reflect the modification of depleted mantle with altered oceanic crust and minor pelagic sediment, or delaminated continental crust, or lithospheric mantle (Escrig et al., 2004; Meyzen et al., 2005; Rehkämper and Hofmann, 1997; Sato et al., 2022). However, the $^{187}Os/^{186}Os$ ratio of the subcontinental lithospheric mantle (SCLM) is relatively lower than that of depleted MORB, which does not support SCLM as the origin of EMI and DUPAL component (Escrig et al., 2004; Hanan et al., 2004). The recycled 1.5Gyr old oceanic crust and pelagic sediment proposed by Rehkämper and Hofmann (1997) are compatible with the lower Pb isotope characteristic of Seg-1 MORBs. However, recycled oceanic crust is a HIMU-type component (Saha et al., 2020), which cannot be noticed in Seg-1 MORBs.

Alternatively, LCC could have been delaminated into the asthenosphere during the break-up of the Gondwana supercontinent, which was probably because of plate tectonic forces localized along weakness zones of thermal erosion of the underplating mantle plume (Bouvet, Marion, and Kerguelen plumes) (Chatterjee et al., 2013; Escrig et al., 2004). Therefore, the delamination of LCC could be the best mechanism for the origin of pyroxenite.

The $^{206}Pb/^{204}Pb$ vs. Fe/Mn co-variation also supports this mechanism, as the lower $^{206}Pb/^{204}Pb$ ratio of Seg-1 indicates the existence of LCC. Seg-1's greater Fe/Mn ratio suggests that the mantle source contains pyroxenite lithology (Fig. 8d). Thus, the origin of pyroxenite in the mantle of Seg-1 can be best attributed to the presence of LCC. The mixing of depleted peridotite-derived melt and minor pyroxenite-derived (LCC) melt can explain the higher apparent melting degree, stronger garnet signature, and lower Pb isotopic ratios of CR Seg-1.

Sato et al. (2022) argued that the DUPAL anomaly of Indian MORB could be explained by a mixture containing partial DMM melt and felsic lower crust-derived melt. The LCC is composed of mafic or felsic granulite, which is more fertile than the peridotite mantle and melts to a higher degree (Escrig et al., 2004; Lee, 2014; Hacker et al., 2015). Combined with the geological evolution, we expect that the delaminated continental crust may act as dispersed pyroxenite materials and plays an essential role in making up the unique Indian Ocean mantle. Additionally, mantle convection may continue to transport the distributed pyroxenite elements, leading to widespread lithological heterogeneity within the MORB source.

5. Conclusions

The new major, trace elements, and Sr-Nd-Pb isotope compositions of MORB from CR Seg-1 were reported and analyzed together with adjacent segments. The lower spreading rate, larger axial depth, and higher mantle Bouguer anomaly of the Seg-1 indicate magma deficiency and a smaller melting degree, which is contradicted by the higher calculated apparent melting degree based on MORB Na_8 and Ca_8/Al_8. This contradiction cannot be reconciled by melting the lithologically homogeneous peridotite mantle but requires lithological heterogeneity.

We proposed that fusible pyroxenite veins exist in the Seg-1 mantle which melts preferably and produces lower Na_8 magma. The prior melting of pyroxenite will cause the mantle to undercool by subtracting latent heat, which in turn limits the melting of peridotite. Higher Zn/Fe and Fe/Mn ratios, the garnet signature revealed by the rare earth elements, and source enrichment evidenced by Sr-Nd-Pb isotopes, all support the presence of a small amount of garnet-pyroxenite in the mantle source. The mixing model of trace elements also shows that Seg-1 MORB may be produced by mixing depleted peridotite-derived and enriched pyroxenite-derived melts. The significant negative correlation between Fe/Mn and $^{206}Pb/^{204}Pb$ indicates that the pyroxene-rich rock may have been transformed from the delaminated LCC. The retained material can be carried on through mantle convection, leading to both widespread lithological and geochemical heterogeneities.

Declaration of Competing Interest

The authors declare that they have no known competing financial interests or personal relationships that could have appeared to influence the work reported in this paper.

Acknowledgments

The samples were all collected from the Chinese research cruises DY28, DY33, and DY57, we are sincerely grateful to all the participating scientists and crew members. This work was supported by funding from the National Key Research and Development Program of China [2021YFF0501301] and the National Natural Science Foundation of China [41872242, 42172231].

Appendix A. Supplementary data

Supplementary data to this article can be found online at https://doi.org/10.1016/j.lithos.2022.106980.

References

Arevalo, R.J., McDonough, W.F., 2008. Tungsten geochemistry and implications for understanding the Earth's interior. Earth Planet. Sci. Lett. 272, 656–665.
Ariskin, A.A., Frenkel, M.Y., Barmina, G.S., Nielsen, R., 1993. COMAGMAT: A FORTRAN program to model magma differentiation processes. Comput. Geosci. 19, 1155–1170.
Armienti, P., Gasperini, D., 2007. Do we really need mantle components to define mantle composition? J. Petrol. 48, 693–709.
Asimow, P.D., Langmuir, C.H., 2003. The importance of water to oceanic mantle melting regimes. Nature. 421, 815–820.
Bodinier, J.L., Garrido, C.J., Chanefo, I., Bruguier, O., Gervilla, F., 2008. Origin of pyroxenite-peridotite veined mantle by refertilization reactions: evidence from the Ronda peridotite (Southern Spain). J. Petrol. 49, 999–1025.
Brunelli, D., Anna, C., Enrico, B., 2018. Thermal effects of pyroxenites on mantle melting below mid-ocean ridges. Nat. Geosci. 11, 520–525.
Cannat, M., Sauter, D., Bezos, A., Meyzen, C., Humler, E., Rigoleur, 2008. Spreading rate, spreading obliquity, and melt supply at the ultraslow spreading Southwest Indian Ridge, Geochemistry, Geophysics. Geosystems. 9, 1–26.
Chatterjee, A., Goswami, A., Scotese, C.R., 2013. The longest voyage: Tectonic, magmatic, and paleoclimatic evolution of the Indian plate during its northward flight from Gondwana to Asia. Gondwana Res. 23, 238–267.
Chen, L., Tang, L.M., Yu, X., Dong, Y.H., 2017. Mantle source heterogeneity and magmatic evolution at Carlsberg Ridge (3.7°N): constrains from elemental and isotopic (Sr, Nd, Pb) data. Mar. Geophys. Res. 38, 47–60.
Collier, J.S., Sansom, V., Ishizuka, O., Taylor, R.N., Minshull, T.A., Whitmarsh, R.B., 2008. Age of Seychelles-India break-up. Earth Planet. Sci. Lett. 272, 264–277.
Coogan, L.A., O'Hara, M.J., 2015. MORB differentiation: in situ crystallization in replenished-tapped magma chambers. Geochim. Cosmochim. Acta 158, 147–161.
Danyushevsky, L.V., 2001. The effect of small amounts of H_2O on crystallisation of mid-ocean ridge and backarc basin magmas. J. Volcanol. Geotherm. Res. 110, 265–280.
Danyushevsky, L.V., Plechov, P., 2011. Petrolog3: integrated software for modeling crystallization processes. Geochem. Geophys. Geosyst. 12, 1–32.
Davis, F.A., Humayun, M., Hirschmann, M.M., Copper, R.S., 2013. Experimentally determined mineral/melt partitioning of first-row transition elements (FRTE) during partial melting of peridotite at 3 GPa. Geochim. Cosmochim. Acta 104, 232–260.
Eason, D., Sinton, J., 2006. Origin of high-Al N-MORB by fractional crystallization in the upper mantle beneath the Galápagos Spreading Center. Earth Planet. Sci. Lett. 252, 423–436.
Escrig, S., Capmas, F., Dupré, B., Allegre, C.J., 2004. Osmium isotopic constraints on the nature of the DUPAL anomaly from Indian mid-ocean-ridge basalts. Nature. 431, 59–63.
Falloon, T.J., Hoernle, K., Schaefer, B.F., Bindeman, I.N., Hart, S.R., Schonberg, D.G., Duncan, R.A., 2022. Petrogenesis of Lava from Christmas Island, Northeast Indian Ocean: Implications for the Nature of Recycled Components in Non-Plume Intraplate Settings. Geosciences. 12, 118.
Gale, A., Dalton, C.A., Langmuir, C.H., Su, Y.J., Schilling, J.G., 2013. The mean composition of ocean ridge basalts. Geochem. Geophys. Geosyst. 14, 489–518.
Gale, A., Langmuir, C.H., Dalton, C.A., 2014. The global systematics of ocean ridge basalts and their origin. J. Petrol. 55, 1051–1082.
Graham, D.W, Hanan, B.B, Hémond, C, Blichert-Toft, J, Albarède, F, 2014. Helium isotopic textures in Earth's upper mantle. Geochem. Geophys. Geosyst 15, 2048–2074.
Hacker, B.R, Kelemen, P.B, Behn, M.D, 2015. Continental lower crust. Annu. Rev. Earth Planet. Sci 43, 050212–123117.
Han, X.Q., Wu, Z.C., Qiu, B.B., 2012. Segmentation of Carlsberg Ridge in Northwest Indian Ocean and its Tectonic and Morphologic Features-the Introduction to the result from DY24 Cruise (in Chinese).
Hanan, B.B., Toft, J.B., Pyle, D.G., Christie, D.M., 2004. Contrasting origins of the upper mantle revealed by hafnium and lead isotopes from the Southeast Indian Ridge. Nature 432, 91–94.
Hart, S.R., 1984. A large-scale isotope anomaly in the Southern Hemisphere mantle. Nature 309, 753–757.
Heinonen, J.S., Luttinen, A.V., Riley, T.R., Michallik, R.M., 2013. Mixed pyroxenite-peridotite sources for mafic and ultramafic dikes from the Antarctic segment of the Karoo continental flood basalt province. Lithos. 177, 366–380.
Herzberg, C., Asimow, P.D., 2008. Petrology of some oceanic island basalts: PRIMELT2. XLS software for primary magma calculation. Geochem. Geophys. Geosyst. 9, 1–25.
Hirschmann, M.M., Stolper, E.M., 1996. A possible role for garnet pyroxenite in the origin of the "garnet signature" in MORB. Contrib. Mineral. Petrol. 124, 185–208.
Hofmann, A.W., 2004. Sampling mantle heterogeneity through oceanic basalts: Isotopes and trace elements. In: Treatise Geochemistry, 2nd ed., pp. 61–101.
Humphreys, E.R., Niu, Y.L., 2009. On the composition of ocean island basalts (OIB): the effects of lithospheric thickness variation and mantle metasomatism. Lithos. 112, 118–136.
Klein, E.M., Langmuir, C.H., 1987. Global correlations of ocean ridge basalt chemistry with axial depth and crustal thickness. J. Geophys. Res. Solid Earth 92, 8089–8115.
Krein, S.B., Behn, M.D., Grove, T.L., 2020. Origins of major element, trace element, and isotope garnet signatures in mid-ocean ridge basalts. J. Geophys. Res. Solid Earth 125, 1–32.
Lambart, S., Laporte, D., Schiano, P., 2009. An experimental study of pyroxenite partial malts at 1 and 1.5 GPa: Implications for the major-element composition of Mid-Ocean Ridge Basalts. Earth Planet. Sci. Lett. 288, 335–347.
Lambart, S., Laporte, D., Schiano, P., 2013. Markers of the pyroxenite contribution in the major-element compositions of oceanic basalts: Review of the experimental constraints. Lithos. 160, 14–36.
Lambart, S., Baker, M.B., Stolper, E.M., 2016. The role of pyroxenite in basalt genesis: Melt-PX, a melting parameterization for mantle pyroxenites between 0.9 and 5 GPa. J. Geophys. Res. 121, 5708–5735.
Large, R.R., Gemmell, J.B., Paulick, H., 2001. A simple approach to understanding the relationship between alteration mineralogy and lithogeochemistry associated with volcanic-hosted massive sulfide deposits. Econ. Geol. 96, 957–971.
Le Roux, V., Lee, C., Turner, S.J., 2010. Zn/Fe systematics in mafic and ultramafic systems: Implications for detecting major element heterogeneities in the Earth's mantle. Geochim. Cosmochim. Acta 74, 2779–2796.
Le Roux, V., Dasgupta, R., Lee, C., 2011. Mineralogical heterogeneities in the Earth's mantle: Constraints from Mn, Co, Ni and Zn partitioning during partial melting. Earth Planet. Sci. Lett. 307, 395–408.
Lee, C., 2014. Physics and chemistry of deep continental crust recycling. In: Treatise on Geochemistry, 2nd ed., pp. 423–456.
Liang, Y., 2020. Trace element fractionation and isotope ratio variation during melting of a spatially distributed and lithologically heterogeneous mantle. Earth Planet. Sci. Lett. 552, 116594.
Liu, Y.S., Gao, S., Kelemen, P.B., Xu, W.L., 2008. Recycled crust controls contrasting source compositions of Mesozoic and Cenozoic basalts in the North China Craton. Geochim. Cosmochim. Acta 72, 2349–2376.
Matzen, A.K., Wood, B.J., Baker, M.B., Stolper, E.M., 2017. The roles of pyroxenite and peridotite in the mantle sources of oceanic basalts. Nat. Geosci. 10, 530–535.
McDonough, W.F, Sun, S.S, 1995. The composition of the Earth. Chem. Geol 120, 223–253.
Melson, W.G., O'Hearn, T., Jarosewich, E., 2003. A data brief on the Smithsonian Abyssal Volcanic Glass Data File. Geochem. Geophys. Geosyst. 3, 1–11.
Meyzen, C.M., Ludden, J.N., Humler, E., Luais, B., Topllis, M.J., Mével, C., Storey, M., 2005. New insights into the origin and distribution of the DUPAL isotope anomaly in the Indian Ocean mantle from MORB of the Southwest Indian Ridge. Geochem. Geophys. Geosyst. 11, 1–34.
Meyzen, C.M., Toft, J.B., Ludden, J.N., Humler, E., Mével, C., Albarède, F., 2007. Isotopic portrayal of the Earth's upper mantle flow field. Nature. 447, 1069–1074.
Michard, A., Albarede, F., 1985. Hydrothermal uranium uptake at ridge crests. Nature. 317, 244–246.
Murton, B.J., Rona, P.A., 2015. Carlsberg Ridge and Mid-Atlantic Ridge: comparison of slow spreading centre analogues. Deep Sea Res. Part II Top. Stud. Oceanogr. 121, 71–84.

Niu, Y.L., 2021. Lithosphere thickness controls the extent of mantle melting, depth of melt extraction and basalt compositions in all tectonic settings on Earth-a review and new perspectives. Earth Sci. Rev. 217, 103614.
Pertermann, M., Hirschmann, M.M., 2003. Partial melting experiments on a MORB-like pyroxenite between 2 and 3 GPa: Constraints on the presence of pyroxenite in basalt source regions from solidus location and melting rate. J. Geophys. Res. 108, 2125.
Pertermann, M., Hirschamnn, M.M., Hametner, K., Gunther, D., Schmidt, M.W., 2004. Experimental determination of trace element partitioning between garnet and silica-rich liquid during anhydrous partial melting of MORB-like eclogite. Geochem. Geophys. Geosyst. 5, 1–23.
Phipps, M.J, 2001. Thermodynamics of pressure release melting of a veined plum pudding mantle. Geochem. Geophys. Geosyst 2, 1–39.
Plank, T., Langmuir, C.H., 1992. Effects of the melting regime on the composition of oceanic crust. J. Geophys. Res. 97, 749–770.
Ray, D., Misra, S., Banerjee, R., 2013. Geochemical variability of MORBs along slow to intermediate spreading Carlsberg-Central Indian Ridge. J. Asian Earth Sci. 70-71, 125–141.
Rehkämper, M., Hofmann, A.W., 1997. Recycled Ocean crust and sediment in Indian Ocean MORB. Earth Planet. Sci. Lett. 147, 93–106.
Rollinson, H.R., 1993. Using Geochemical Data: Evaluation, Presentation, Interpretation. Press Cambridge University, London, pp. 1–384.
Rudnick, R.L., Gao, S., 2003. Composition of the Continental Crust. Treatise Geochem. 1–64.
Saha, A., Sensarma, S., Hazre, A., Ganguly, S., Peketi, A., Doley, B., Mudholkar, A.V., 2020. Imprints of ancient recycled oceanic lithosphere in heterogeneous Indian Ocean mantle: evidence from petrogenesis of Carlsberg ridge basalts from Northwest Indian Ocean. Gondwana Res. 86, 60–82.
Russo, C.J, Rubin, K.H, Graham, D.W, 2009. Mantle melting and magma supply to the Southeast Indian Ridge: The roles of lithology and melting conditions from U-series disequilibria. Earth Planet. Sci. Lett 278, 55–66.
Saha, A., Hazre, A., Santosh, M., Ganguly, S., Li, S.S., Manikyamba, C., 2021. Episodic recycling of ancient metasomatized continental lithosphere: evidence from lower oceanic crust of the Central Indian Ridge. Lithos. 400–401.
Salters, V.J.M., Dick, H.J.B., 2002. Mineralogy of the mid-ocean-ridge basalt source from neodymium isotopic composition of abyssal peridotites. Nature 418, 68–72.
Salters, V.J.M., Hart, S.R., 1989. The hafnium paradox and the role of garnet in the source of mid-ocean-ridge basalts. Nature. 342, 420–422.
Salters, V.J.M., Stracke, A., 2004. Composition of the depleted mantle. Geochemistry: Geophysics. Geosystems. 5, 1–27.
Sato, H., Machida, S., Ashida, K., Senda, R., Nakamura, K., Yoneda, S., 2022. Unradiogenic lead isotopic signatures of the source mantle beneath the southernmost segment of the Central Indian Ridge. Lithos. 424–425.
Shaw, D.M., 1970. Trace element fractionation during anatexis. Geochim. Cosmochim. Acta 34, 237–243.
Shen, Y., Forsyth, D.W., 1995. Geochemical constraints on initial and final depths of melting beneath mid-ocean ridges. J. Geophys. Res. Solid Earth 100, 2211–2237.
Sobolev, A.V., Hofmann, A.W., Kuzmin, D.V., Yaxley, G.M., Arndt, N.T., Chung, S.L., Danyushevsky, L.V., Elliott, T., Frey, F.A., Garcia, M., Gurenko, A., Kamenetsky, V.S., Kerr, A.C., Krivolutskaya, A.N., Matvienkov, V., Nikogosian, I.K., Rocholl, A., Sigurdsson, I.A., Sushchevskaya, N.M., Teklay, M., 2007. The amount of recycled crust in sources of mantle-derived melts. Science. 316, 412–417.
Standish, J.J., Dick, H.J.B., Michael, P.J., Melson, W.G., O'Hearn, T., 2008. MORB generation beneath the ultraslow spreading Southwest Indian Ridge (9°-25°E): Major element chemistry and the importance of process versus source. Geochem. Geophys. Geosyst. 9, 1–39.
Stracke, A., Bernard, B., 2008. The importance of melt extraction for tracing mantle heterogeneity. Geochim. Cosmochim. Acta 73, 218–238.
Sun, S.S., McDonough, W.F., 1989. Chemical and isotopic systematics of oceanic basalts: Implications for mantle composition and processes. Geol. Soc. Lond. Spec. Publ. 42, 313–345.
Wang, S, Zhang, G.L, 2022. Geochemical constraints on source nature and recycled oceanic crust in the mantle of the Celebes Sea. Lithos 418, 1–12.
Warren, J.M., Shimizu, N., Sakaguchi, C., Dick, H.J.B., Nakamura, E., 2009. An assessment of upper mantle heterogeneity based on abyssal peridotite isotopic compositions. J. Geophys. Res. 114, 1–36.
Weaver, J.S., Langmuir, C.H., 1990. Calculation of phase equilibrium in mineral-melt systems. Comput. Geosci. 16, 1–19.
White, W.M., 2015. Isotopes, DUPAL, LLSVPs, and Anekantavada. Chem. Geol. 419, 10–28.
Workman, R.K., Hart, S.R., 2005. Major and trace element composition of the depleted MORB mantle (DMM). Earth Planet. Sci. Lett. 231, 53–72.
Yang, S.Y., Humayun, M., Salters, V.J.M., 2020. Elemental constraints on the amount of recycled crust in the generation of mid-oceanic ridge basalts (MORBs). Sci. Adv. 6, 1–12.
Yu, X., Han, X.Q., Qiu, Z.Y., Wang, Y.J., Tang, L.M., 2019. Definition of Northwest Indian Ridge and its Geologic and Tectonic Signature. Earth Sci. 44, 626–639.
Zhang, G.L., Zong, C.L., Yin, X.B., Li, H., 2012. Geochemical constraints on a mixed pyroxenite-peridotite source for East Pacific rise basalts. Chem. Geol. 330-331, 176–187.
Zong, T, Han, X.Q, Liu, J.Q, Wang, Y.J, Qiu, Z.Y, Li, H.L, Yu, X, 2019. H_2O in basaltic glasses from the slow-spreading Carlsberg Ridge: Implications for mantle source and magmatic processes. Lithos 331, 176–187.
Zong, T., Han, X.Q., Liu, J.Q., Wang, Y.J., Qiu, Z.Y., Yu, X., 2020. Fractional crystallization processes of magma beneath the Carlsberg Ridge (57°-65°E). J. Oceanol. Limnol. 38, 75–92.